Selected Topics of Semiconductor Physics and Technology

Ausgewählte Probleme der Halbleiterphysik und Technologie

Vol. 135

Stefan Birner

Modeling of semiconductor nanostructures and semiconductor–electrolyte interfaces

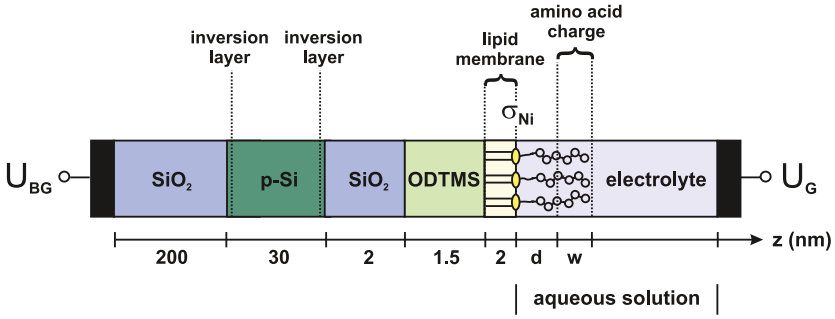

S. Birner • Modeling of semiconductor–electrolyte interfaces

ISBN 978-3-941650-35-0

(€ 18,00)

135

Editors:

G. Abstreiter, M.-C. Amann, M. Stutzmann, P. Vogl

Walter Schottky Institut, Technische Universität München

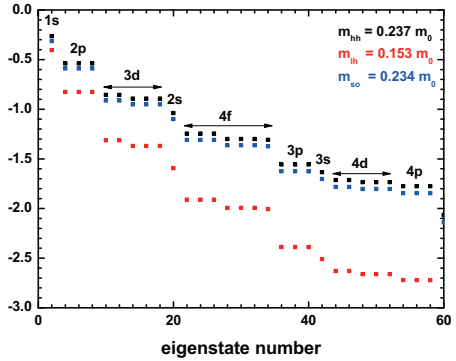

Figure 3.7.: Hole energy levels of a spherical silicon quantum dot ('artificial atom') of diameter 5 nm for heavy (black squares), light (red squares) and split-off holes (blue squares) calculated with the single-band Schrödinger equation. The degeneracies of the levels are indicated by the standard atomic orbital notation known from the electron configuration of atoms.

where R is the radius of the sphere and $m_\mathrm{h} = -0.237 m_0$ is the isotropic hole mass for our choice of parameters with the minus sign for the hole mass indicating that the dispersion in the bulk material is bent downwards. The calculated value for the ground state energy $E_1 = -0.254\,\mathrm{eV}$ is close to our numerical value of $-0.237\,\mathrm{eV}$ using the 6×6 $\mathbf{k}\cdot\mathbf{p}$ method. Burdov writes down eq. (3.163) without the free electron term '+1' which is overall consistent within their article but their parameters [Bur02] are unfortunately incorrect. The parameters given in eq. (3.161) which are derived from the Luttinger parameters of Lawaetz [Law71] are the correct ones whereas the parameters termed L and M in Burdov's article are actually the L^LK and M^LK parameters (eq. (3.33), eq. (3.34)). Thus they have to be corrected by '+1', i.e. $L^\mathrm{LK} = -5.8\frac{\hbar^2}{2m_0}$ and $M^\mathrm{LK} = -4.43\frac{\hbar^2}{2m_0}$ would have been the correct values to be consistent within their article (see also the discussion on the different and thus confusing definitions of the L and M parameters in Section 3.1). Consequently, their calculated hole mass of $m_\mathrm{h} = -0.19 m_0$ has to be corrected by our value of $m_\mathrm{h} = -0.237 m_0$.

For comparison, the results of the single-band calculations with isotropic heavy, light and split-off hole masses are shown in Fig. 3.7 for the same quantum dot. Here, each state is twofold degenerate due to spin but only one of these two energy levels is shown. The numbering of the horizontal axis, however, is taking spin into account. Figure 3.6 shows the lowest 60 eigenvalues. This numbering corresponds roughly to the first 20

eigenvalues for each hole species in Fig. 3.7. The degeneracies of the levels are indicated by the standard atomic orbital notation known from the electron configuration of atoms ($1s$, $2p$, $3d$, $2s$, $4f$, ...). From that labeling it becomes clear why quantum dots are termed 'artificial atoms'. In contrast to real atoms, their energy levels can be tuned to match technologically relevant energy regimes, while showing qualitatively similar energy spectra as atoms, at least for spherical dots. Self-organized quantum dots, however, are mainly showing an energy spectrum similar to a two-dimensional harmonic oscillator as their confinement potential in the plane perpendicular to the growth direction can often be approximated by a parabolic confinement (see also the discussion in Subsection 2.3.1). The fivefold degeneracy of the d levels and the sevenfold degeneracy of the f level is not reproduced well because the ideal shape of the spherical QD is approximated by a QD discretized on a rectangular grid having cubic symmetry. Obviously, the numerical single-band results are very poor in comparison to the $\mathbf{k}\cdot\mathbf{p}$ results with the exception of the ground state energy $E_1 = -0.265\,\mathrm{eV}$.

We have verified that both the next**nano**[3] and the next**nano**++ software lead to the same $\mathbf{k}\cdot\mathbf{p}$ eigenvalue spectrum (not shown). For both, we used a cuboidal shaped quantum region although next**nano**[3] is capable of using arbitrarily shaped quantum regions, e.g. a spherical quantum region which is numerically more efficient as less quantum grid points are needed. If m grid points can be excluded from the quantum region due to an optimal choice of quantum region shape, the dimension N of the 6×6 $\mathbf{k}\cdot\mathbf{p}$ matrix reduces to $N - 6m$.

For this particular spherical geometry, the eigenvalues are highly degenerate, not only due to spin but also due to geometry. This sometimes causes problems for certain eigenvalue solvers as they might miss some of these degenerate eigenvalues. For instance, our implementation of the Arnoldi method that uses Chebyshev polynomials as preconditioner [TZA+06] missed some degenerate eigenvalues. For this reason it is of great advantage if any numerical software has redundancy in terms of several eigensolvers, where one can choose from, in order to check results for consistency and accuracy, as well as performance. The ARPACK eigenvalue solver [LSY98] took around 6 minutes for 60 eigenvectors where the dimension of the matrix was $N = 55566$ corresponding to $21\times21\times21 = 9261$ grid points with a grid resolution of 0.25 nm in each direction.

3.5. Type-III broken-gap band alignment – HgTe–CdTe quantum well

HgTe is an interesting material for studies of the intrinsic spin Hall effect [BRN+10] and the quantum spin hall effect [BHZ06], or spin splitting effects in general due to its large Rashba-type spin-orbit splitting. HgTe is a zero-gap semiconductor that can be embedded between CdTe layers to form a HgTe–CdTe quantum well (QW) heterostructure which shows an interesting type-III band alignment where the valence band edge in the HgTe QW lies above its conduction band edge. Due to this band alignment it is not possible to apply a single-band Hamiltonian. Thus a $\mathbf{k}\cdot\mathbf{p}$ or tight-binding approach is required. Large HgTe quantum wells have an inverted band structure where the highest

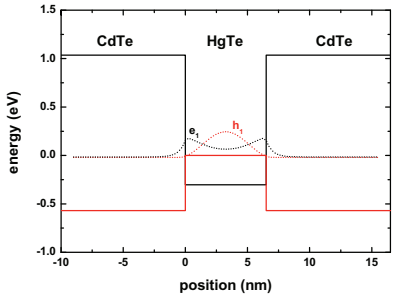

Figure 3.8.: Probability density of the lowest electron (e_1) and highest hole (h_1) eigenstates of a 6.5 nm HgTe quantum well calculated with the $\mathbf{k}\cdot\mathbf{p}$ method. In the $\mathbf{k}\cdot\mathbf{p}$ method, the eigenstates correspond to envelope functions. The conduction (black solid line) and valence band edges (red solid line) form a type-III band alignment.

hole state (h_1) lies above the lowest electron state (e_1). For smaller quantum well widths, the quantum confinement increases and below a critical well width, the band structure becomes normal again with the electron state above the hole state. Figure 3.8 shows the square of the calculated $\mathbf{k}\cdot\mathbf{p}$ wave functions of e_1 and h_1 at the crossover well width at 6.5 nm. Increasing the well width shifts the e_1 state below the h_1 state. This is shown in Fig. 3.9 where the probability density of the relevant states have been calculated with the empirical tight-binding method for a 7.8 nm HgTe quantum well. One can nicely see that in the tight-binding method the envelope of the probability density corresponds to $\mathbf{k}\cdot\mathbf{p}$ envelope functions. For the $sp^3d^5s^*$ tight-binding [JSBB98] calculations, we used a valence band offset of 0.4 eV. For the $\mathbf{k}\cdot\mathbf{p}$ calculations, we took exactly the same material parameters as in Ref. [NPJJ+05], including their valence band offset of 0.570 eV. In both cases, we neglected strain effects for simplicity.

Figure 3.10 shows the energies of the electron and hole states in a HgTe–CdTe quantum well as a function of HgTe QW width calculated with the 8×8 $\mathbf{k}\cdot\mathbf{p}$ method. The crossover of normal to inverted band structure occurs around 6.5 nm and corresponds to the situation in Fig. 3.8. The dashed lines indicate the energetic positions of the conduction and valence band edges of the HgTe QW. Our results for the crossover width are in good agreement to the calculations of Novik et al. [NPJJ+05], and also close to tight-binding calculations [CST].

I have implemented Peter Vogl's TIGHTEN superlattice code into the next**nano**^{3} software package, so that it is now more convenient to perform systematic comparisons between the $\mathbf{k}\cdot\mathbf{p}$ and the tight-binding method for quantum wells.

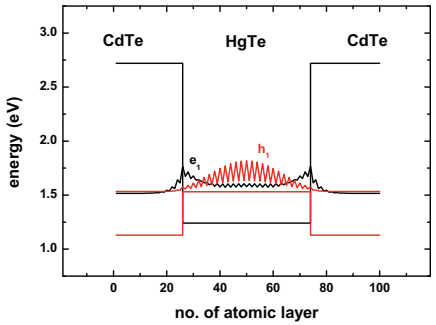

Figure 3.9.: Probability density of the lowest electron (e_1) and highest hole (h_1) eigenstates of a 7.8 nm HgTe quantum well calculated with the empirical tight-binding method.

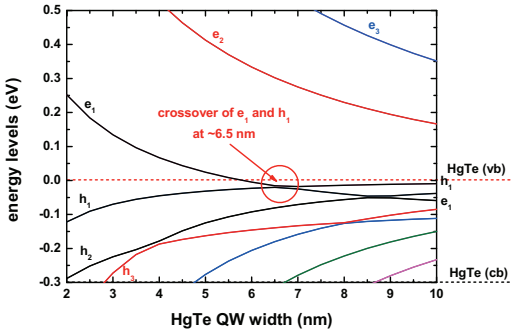

Figure 3.10.: Calculated energies of the electron and hole states in a HgTe–CdTe quantum well as a function of HgTe QW width (8×8 $\mathbf{k}\cdot\mathbf{p}$). The crossover of normal to inverted band structure occurs around 6.5 nm and corresponds to the situation in Fig. 3.8. The dashed lines indicate the conduction and valence band edges of the HgTe QW.